# Control of the hierarchical self-assembly of polyoxometalate-based metallomacrocycles by redox trigger and solvent composition

Madeleine Piot[a], Benjamin Abécassis[b,c,1], Dalil Brouri[d], Claire Troufflard[a], Anna Proust[a], and Guillaume Izzet[a,1]

[a]Institut Parisien de Chimie Moléculaire, CNRS, Sorbonne Université, F-75005 Paris, France; [b]Laboratoire de Physique des Solides, CNRS, UMR 8502, Université Paris-Saclay, Université Paris-Sud, 91405 Orsay, France; [c]Laboratoire de Chimie, Ecole Normale Supérieure de Lyon, CNRS, UMR 5182, Université Claude Bernard, Université de Lyon, 69007 Lyon, France; and [d]Laboratoire de Réactivité de Surface, CNRS, Sorbonne Université, F-75005 Paris, France

Edited by Thomas E. Mallouk, The Pennsylvania State University, University Park, PA, and approved August 1, 2018 (received for review May 16, 2018)

**Discrete metallomacrocycles are attractive scaffolds for the formation of complex supramolecular architectures with emergent properties. We herein describe the formation of hierarchical nanostructures using preformed metallomacrocycles by coordination-driven self-assembly of a covalent organic–inorganic polyoxometalate (POM)-based hybrid. In this system, we take advantage of the presence of charged subunits (POM, metal linker, and counterions) within the metallomacrocycles, which drive their aggregation through intermolecular electrostatic interactions. We show that the solvent composition and the charge of the metal linker are key parameters that steer the supramolecular organization. Different types of hierarchical self-assemblies, zero-dimensional (0D) dense nanoparticles, and 1D worm-like nanoobjects, can be selectively formed owing to different aggregation modes of the metallomacrocycles. Finally, we report that the worm-like structures drastically enhance the solubility in water of a pyrene derivative and can act as molecular carriers.**

polyoxometalates | hierarchical self-assembly | organic–inorganic hybrids | SAXS | molecular carrier

A wide range of structures and functions observed in natural systems involves hierarchical self-assembly processes (1). In search of innovative soft materials, chemists have devoted important efforts to develop artificial multiscale systems with controlled structures and shapes (2–8). Tracking this challenging synthetic issue should open new perspectives to elaborate supramolecular architectures with advanced properties. For instance, the emergence of novel properties often arises when a certain level of structural complexity is reached from components of lower complexity (9). The construction of hierarchical supramolecular architectures can be achieved following a stepwise synthetic strategy relying on the design of a preassembled structural motif that can further self-assemble into more complex nanostructures through additional noncovalent interactions (10). Owing to their high strength, metal coordination and electrostatic interactions are well suited for the design of hierarchical supramolecular architectures. Metal coordination is a powerful route for controlling the topology of the desired supramolecular architectures by using suitable metallic ions and ligands (11, 12). Regarding electrostatic interactions, they play crucial roles in biological systems in recognition processes and are (among other) involved in maintaining (natural and synthetic) nanoassemblies (6, 13, 14). While the combination of these interactions is at the base of a variety of coordination polymers with controlled orders (4, 15, 16), the use of metallomacrocycles, as building blocks, for the construction of complex hierarchical architectures through electrostatic interactions remains poorly explored (17–19). In this context, we previously reported the metal-directed self-assembly of polyoxometalate (POM)-based hybrids in which the POM is covalently bonded to two remote binding sites (20–22). POMs are polyanionic nanosized molecular metal-oxo clusters that provide original molecular building units for the elaboration of multifunctional materials (23, 24). While the reaction of bis(pyridine)-terminated hybrids with a neutral metal linker (*trans*-$[PdCl_2(CH_3CN)_2]$) mostly leads to the formation of metallomacrocycles (triangle and square) (20, 22), the coordination-driven self-assembly of a bis(terpyridine)-terminated hybrid in the presence of a cationic metal linker ($Fe^{2+}$) provided different supramolecular organizations according to the solvent composition. In this system, discrete metallomacrocycles combining negatively charged POMs, cationic metal linkers, and tetrabutyl ammonium (TBA) counterions, are only observed in DMSO (i.e., a strongly dissociating solvent) as a consequence of intermolecular interactions weaker than the solvation energy. By contrast, in acetonitrile (i.e., a less-dissociating solvent), the metallomacrocycles act as secondary building units and self-assemble through combination of intermolecular electrostatic interactions (between the charged components) into dense nanoobjects of ∼8-nm diameter. This system is an example of controlled assembly of POM-based building blocks to dense nanoparticles with multiple levels of organization, entirely governed by the solvent composition. On the basis of these results, we wondered whether we could control the shape of the hierarchical nanostructures through the modification of the charge of the metal linker and/or the nature of the additional solvent inducing the aggregation. We herein describe the formation of supramolecular nanoassemblies with worm-like structures, resulting from a different organization of the preformed

## Significance

Hierarchical self-assembly is a powerful route allowing the elaboration of complex supramolecular architectures with emergent structuration or properties. Starting from well-defined molecular building units, this synthetic strategy relies on the construction of a preassembled structural motif that can further self-assemble through additional noncovalent interactions. In this context, we developed a system based on a covalent organic–inorganic polyoxometalate hybrid building block combining metal-driven self-assembly and electrostatic interactions. We herein show that in this system, the supramolecular organization can be controlled by a redox stimulus and/or the solvent composition giving rise to various types of nanoarchitectures from discrete metallomacrocycles to 1D worm-like nanoobjects.

Author contributions: G.I. designed research; M.P. and B.A. performed research; B.A., D.B., and C.T. contributed new reagents/analytic tools; M.P., B.A., C.T., A.P., and G.I. analyzed data; and G.I. wrote the paper.

The authors declare no conflict of interest.

This article is a PNAS Direct Submission.



[1]To whom correspondence may be addressed. Email: benjamin.abecassis@ens-lyon.fr or guillaume.izzet@sorbonne-universite.fr.

This article contains supporting information online at www.pnas.org/lookup/suppl/doi:10.1073/pnas.1808445115/-/DCSupplemental.

Published online August 21, 2018.

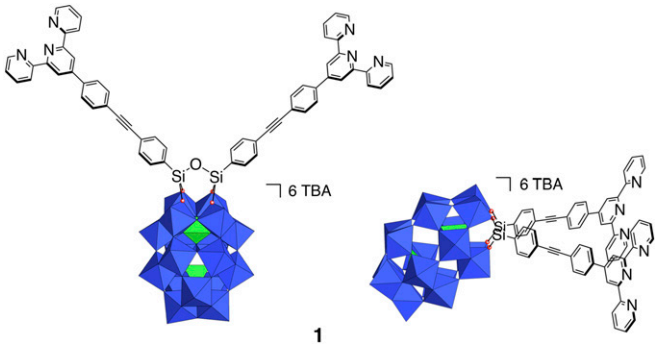


**Fig. 1.** Schematic molecular representations of the hybrid **1** (derived from an energy-minimized structure) from two different viewpoints. Color code: $WO_6$ octahedra, blue; $PO_4$ tetrahedra, green.

POM-based metallomacrocycles through the increase of the cation linker charge. We also show that these worm-like nanostructures also form in DMSO/water mixtures. We thus report that using a single molecular building unit different supramolecular organizations can be obtained according to the redox state of the metal linker (+2 and +3) and the solvent composition (DMSO, DMSO/MeCN, DMSO/$H_2O$). Finally, we show that these nanoaggregates drastically enhance the solubility in water of a pyrene derivative and can thus act as molecular carriers.

## Results and Discussion

**Complexation of the POM-Based Building Block to $[Co(H_2O)_6](NO_3)_2$.** The starting POM-based building block $(TBA)_6[P_2W_{17}O_{61}\{O(SiC_{29}H_{18}N_3)_2\}]$ denoted **1** contains two terpyridine (tpy) units connected to the lacuna of the Dawson-type POM $\alpha_2$-$[P_2W_{17}O_{61}]^{10-}$ through a Si-O-Si anchorage (Fig. 1). Organosilyl derivatives of monovacant lacunary POMs, either in the Keggin (i.e., $[PW_{11}O_{39}\{O(SiR)_2\}]^{3-}$) or Dawson (i.e., $[P_2W_{17}O_{61}\{O(SiR)_2\}]^{6-}$) series display very similar structures with orthogonal organic arms (25–27). Density functional theory calculations of **1** converged to an energy-minimized structure in which the angle between the arms was slightly higher (~97°) (21). In our previous study (21), the metal-directed self-assembly of this hybrid was performed using Fe(II) salts since the Fe(II) bis(terpyridine) complexes are diamagnetic (which facilitates NMR characterization) and display high stability. Upon the addition of one equiv of $[Fe(H_2O)_6](ClO_4)_2$ onto **1** in DMSO-$d_6$, a single set of rather broad signals was observed in $^1$H NMR spectroscopy, suggesting the formation of a unique cyclic oligomeric species (21). We assumed the formation of a molecular triangle by analogy to the reaction of the closely related bis(pyridine)-terminated Dawson-based system with *trans*-$[PdCl_2(CH_3CN)_2]$ (22). The oxidation of Fe(II) bis(terpyridine) occurs at high potential (28) owing to the high stability of the low-spin $t_{2g}^6$ electron configuration of Fe(II). On the counterpart, Co(II) bis(terpyridine) complexes can be much more easily oxidized (28, 29) since the resulting Co(III) bis(terpyridine) complexes display the stable low-spin $t_{2g}^6$ electron configuration. This drove us to study the coordination-driven self-assembly of **1** with Co(II) salts with the aim of triggering the supramolecular organization by the redox state of the linking metal. The incremental addition of $[Co(H_2O)_6](NO_3)_2$ to a solution of **1** (1 mM in DMSO-$d_6$) up to ~0.5 equiv. mostly leads to the appearance of a single set of signals in the $^1$H low-field region (above 10 ppm) attributed to coordinated terpyridine units (Fig. 2). In the following we define the composition by the parameter $\rho = c_{Co}/c_{POM}$. For $0.5 < \rho < 1$, this set of signals splits into two sets. When $\rho = 1$, the signals of the starting parent hybrid have disappeared, suggesting that the formed species display a POM:Co(II) 1:1 stoichiometry. The monitoring of the addition of $[Co(H_2O)_6](NO_3)_2$ to **1** by $^{31}$P NMR also indicates the initial formation of a single set of signals (−12.7 and −9.7 ppm), for $0 < \rho < 0.5$, close to those of the initial hybrid and attributed to the distal and proximal phosphorus atoms (with respect to the lacuna of the parent POM), respectively (*SI Appendix*, Fig. S1). When $\rho = 1$ the resulting species displays a broad peak at −12.6 ppm and two peaks, −9.55 and −9.6 ppm. Note that for $0.5 < \rho < 1$, all $^{31}$P NMR signals are observed, indicating the presence of a mixture of all species at this stage of the complexation. A variable temperature $^1$H NMR study of a solution of **1** (1 mM in DMSO-$d_6$) with $\rho = 1$ in the 300–350-K range reveals that the ratio in peak intensity between the two sets of signals is significantly affected by the temperature (Fig. 3 and *SI Appendix*, Fig. S2). The minor set of signals at room temperature (represented in blue in Fig. 3) further decreases in intensity upon warming to 350 K. Note that, at each temperature, a long time is necessary (a few hours for temperature just above 300 K) so that the equilibrium is reached. Similarly, when decreasing the temperature from 350 to 300 K, it takes 1 d so that the relative intensity between the two sets of signals becomes similar to that of the spectrum before heating. All these findings indicate sluggish kinetics processes. To complete the characterization of the discrete supramolecular assemblies, we performed small-angle X-ray scattering (SAXS) experiments on solutions of **1** in DMSO-$d_6$ before and after the addition of 1 equiv of $[Co(H_2O)_6](NO_3)_2$ (*SI Appendix*, Fig. S4). SAXS is a very powerful technique that we and others have successfully used to characterize nanosized metal-oxo clusters (23, 30, 31). The SAXS patterns of a solution of the molecular building-block **1** (1 mM in DMSO-$d_6$) with $\rho = 1$ are very similar to those, previously reported, for the coordination-driven self-assembly of **1** with $[Fe(H_2O)_6](ClO_4)_2$. These SAXS signals display similar oscillations located at $q > 0.1$ Å$^{-1}$ (corresponding to POM-to-POM distances within the discrete supramolecular species) and same increase in intensity (neglecting the decrease in intensity when $q \to 0$ caused by the electrostatic interactions) compared with that of the molecular building-block **1** in the low-q region. This indicates that similar discrete supramolecular species are formed in DMSO-$d_6$ either with $[Co(H_2O)_6](NO_3)_2$ or $Fe(H_2O)_6](ClO_4)_2$. The formation of a unique set of $^1$H NMR signals at intermediate concentration of metal linker (i.e., for $0.5 < \rho < 1$) that splits into two sets of signals upon the addition of 1 equiv of Co(II) per POM is similar to the behavior of a bis(pyridine)-terminated Keggin-based hybrid analog in the

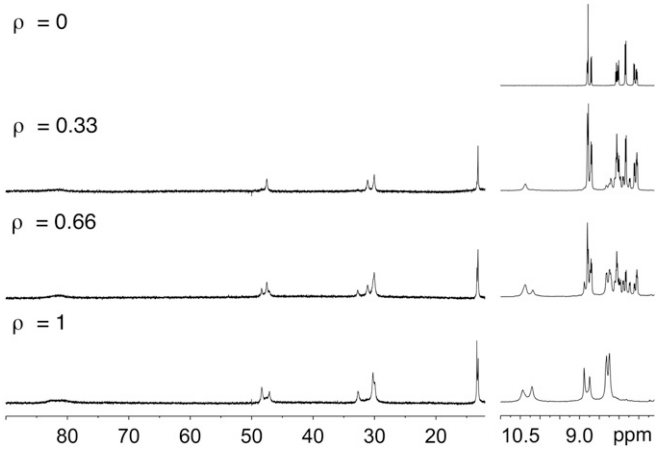


**Fig. 2.** Evolution of the $^1$H NMR (DMSO-$d_6$, 400 MHz) spectrum of a solution **1** (1 mM) upon the progressive addition of $[Co(H_2O)_6](NO_3)_2$. Note that for sake of clarity the intensity of paramagnetic region (12–90 ppm) was expanded.

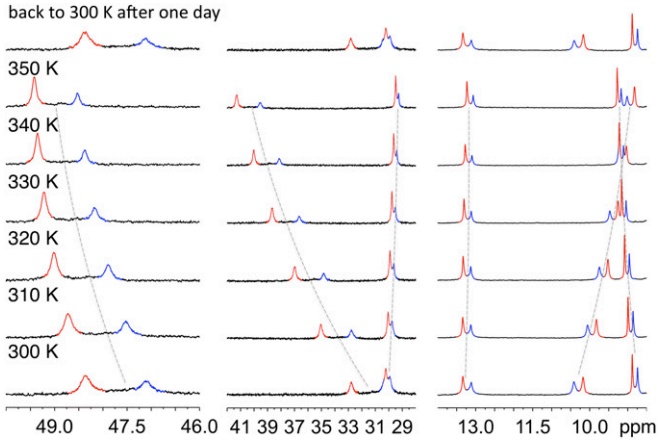


**Fig. 3.** Evolution of the $^{1}$H NMR (DMSO-$d_6$, 400 MHz) spectrum of a solution of **1** (1 mM) in the presence of 1 equiv of $[Co(H_2O)_6](NO_3)_2$ upon temperature modification. The signals outlined in red and blue are attributed to those of the molecular triangles and square, respectively.

presence of *trans*$[PdCl_2(CH_3CN)_2]$ (20). In this last system we observed the prior formation of a molecular dimer at intermediate concentration of metal linker, which evolves into molecular triangle and square in the presence of 1 equiv of metal linker. We concluded that the formation of the cyclic assembly in such system is a noncooperative process probably owing to a high entropic cost due to the global gathering of the associated counterions (20). In the present case, the presence of two sets of $^{1}$H and $^{31}$P signals for POM:Co(II) 1:1 stoichiometry can be attributed either to the presence of different isomers (displaying different orientations of the POM units with respect to the plane defined by the Co(II) centers) or to the formation of different cyclic oligomers (i.e., a triangle and a square). The fact that the ratio between the two sets of signals is noticeably affected by the temperature rules out the first hypothesis and can only be explained by the presence of metallomacrocycles of different nuclearities. Since the formation of a cyclic tetramer vs. a trimer is entropically unfavorable we assign the minor $^{1}$H NMR signals to the molecular square (Fig. 3). As in the bis(pyridine)-terminated Keggin-based system, the observation of a single set of signals at intermediate Co(II) concentration indicates that a molecular dimer with a POM:Co(II) 2:1 stoichiometry forms prior the discrete metallomacrocycles (Fig. 4). As previously mentioned, we observed a single set of signals when 1 equiv of $[Fe(H_2O)_6](ClO_4)_2$ was added to **1** (21). Considering that Fe(II) and Co(II) bis(terpyridine) complexes display same structure and charge it is very likely that coordination-driven self-assembly of **1** with Fe(II) and Co(II) would lead to similar supramolecular species. Note that in the previously reported **1.Fe$^{II}$** system (in the following, **1.M$^{n}$** stands for the supramolecular species displaying a 1:1 stoichiometry between the POM and the metal linker) we observed that the perchlorate ions are not associated with the metallomacrocycle (21), which is further confirmed by SAXS. While we initially proposed that in the **1.Fe$^{II}$** system only triangles metallomacrocycles are formed, the current study suggests that molecular squares are also present, albeit in smaller quantity (Fig. 4). Note that because of the paramagnetism of Co(II) ions, we were not able to calculate the diffusion coefficient of the different Co(II)-containing species. However, we succeeded in evaluating the $T_2$ relaxation time of selected signals of both species (*SI Appendix*, Fig. S3). We observed that the signals of the molecular square have a shorter $T_2$ than those of the triangle as expected for bigger species (transverse relaxation is known to be faster for large molecules for which Brownian motions are slower).

**Oxidation of the Co(II) Centers with Tribromide.** The addition of tetrabutyl ammonium tribromide (1 equiv, 20 mM in DMSO-$d_6$) to a DMSO-$d_6$ solution containing **1.Co$^{II}$** leads to a rapid fading of the solution color from bright orange to the characteristic yellow color of the low-spin Co(III) bis(terpyridine) complex, the process being complete in a few minutes. The $^{1}$H NMR spectrum of the resulting species displays ill-defined signals in the aromatic region, while no signal are observed above 10 ppm, indicating the absence of paramagnetic species (*SI Appendix*, Fig. S5). Similarly, the $^{31}$P NMR spectrum of the solution displays a set of very broad signals at −9.7 and −12.8 ppm (*SI Appendix*, Fig. S1). Finally, SAXS intensity in the low-q region of the solution after oxidation of the Co(II) centers is enhanced by a factor of ∼4.5 (*SI Appendix*, Fig. S4). From the Guinier regime of SAXS curve (32), we can extract a radius of gyration $r_g$ = 2.8 nm for the

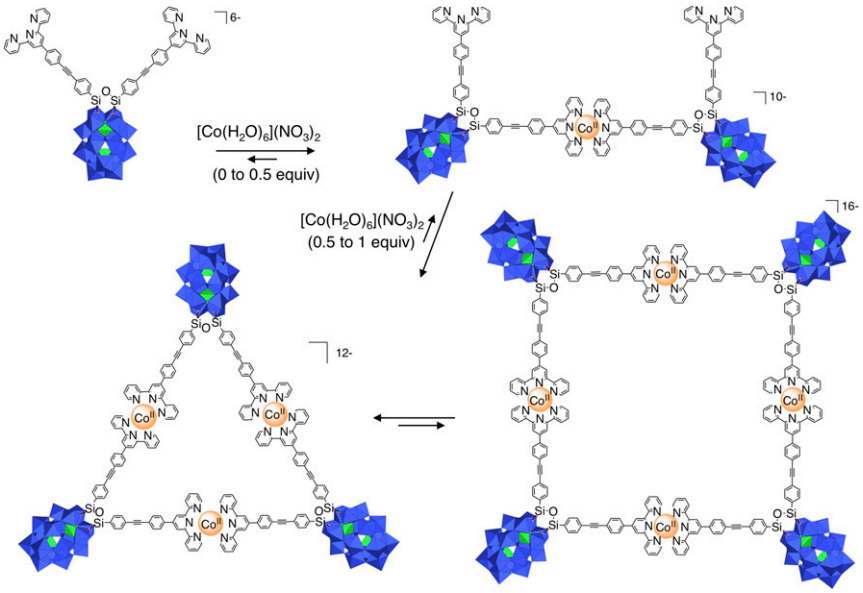


**Fig. 4.** Metal-driven formation of the molecular triangle and square from **1** in DMSO-$d_6$.

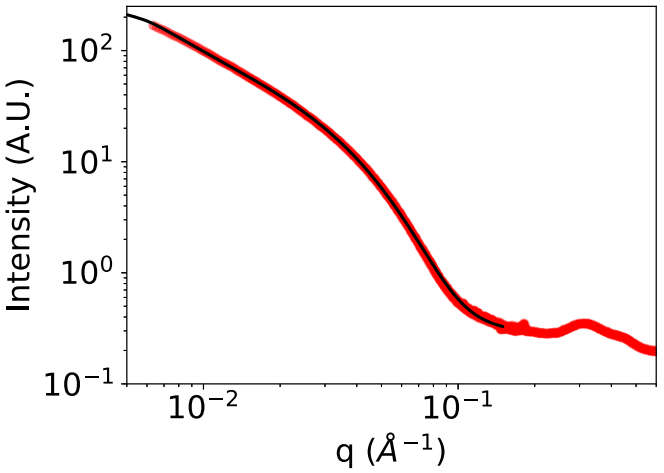


**Fig. 5.** Comparison of the experimental SAXS pattern of **1.Co$^{III}$** (red) in DMSO-$d_6$/$CD_3CN$ (1:4, vol/vol) to the theoretical SAXS intensity (computed using SasView) (36) of a flexible cylinder of 94 nm in length, 3.4 nm in radius (polydispersity 35%) and a Kuhn length of 51 nm (black).

assemblies of **1.Co$^{III}$** in DMSO-$d_6$. These features indicate the formation of aggregated species. In the **1.Fe$^{II}$** system, the aggregation of the discrete metallomacrocycle was achieved through the change of the composition of the solvent (21). Upon the dilution of the preformed metallomacrocycles with acetonitrile (i.e., a less-dissociating solvent than DMSO), the solvation energy of the metallomacrocyles becomes weaker than the electrostatic interactions, which forces their aggregation into dense nanoobjects. In the present case, aggregation is induced by an increase in the electrostatic interactions through the modification of the charge of the metal linker. The solvent composition and the redox state of the metal linker are thus two control levers of the formation of the hierarchical supramolecular assemblies based on the POM-based building unit **1**.

**Modification of the Solvent Composition: DMSO-MeCN Mixture.** The effect of the addition of $CD_3CN$ to DMSO-$d_6$ solutions of **1.Co$^{II}$** and **1.Co$^{III}$** was investigated by SAXS. For these experiments concentrated solutions of **1.Co$^{II}$** and **1.Co$^{III}$** ($c_{POM}$ = 5 mM) in DMSO-$d_6$ were prepared before their dilution with $CD_3CN$ or DMSO-$d_6$. The signal intensity in the low-q region of a solution of **1.Co$^{II}$** ($c_{POM}$ = 1 mM) in a DMSO-$d_6$/$CD_3CN$ (1:4, vol/vol) mixture is significantly higher (by a factor of 12.3) than that of **1.Co$^{II}$** in DMSO-$d_6$ (for the same concentration), which suggests the presence of nanoaggregates similar to those described with the **1.Fe$^{II}$** system (*SI Appendix*, Fig. S4). From the Guinier regime of SAXS curve, we can extract a radius of gyration of 3.7 nm for the aggregates of **1.Co$^{II}$** in the DMSO-$d_6$/$CD_3CN$ (1:4, vol/vol) mixture, which is similar to the value found for **1.Fe$^{II}$**. As regards the **1.Co$^{III}$** system, SAXS patterns of a DMSO-$d_6$/$CD_3CN$ (1:4, vol/vol) mixture of the species ($c_{POM}$ = 1 mM) display unusual features. While the signals of the aggregated species of **1.Co$^{II}$** in DMSO-$d_6$/$CD_3CN$ (1:4, vol/vol) and **1.Co$^{III}$** in DMSO-$d_6$ reach a plateau in the low-q region, indicative of zero-dimensional nanoobjects, the SAXS intensity of **1.Co$^{III}$** in DMSO-$d_6$/$CD_3CN$ (1:4, vol/vol) keeps increasing for $q \to 0$ with a slope of $\sim q^{-1}$. This suggests that the aggregated species are rod-shaped. In the low-q region, these SAXS patterns can be very well reproduced by a model of flexible cylinders measuring 94 nm in length and 3.4 nm in radius (35% polydispersity) and a Kuhn length (i.e., average segment length of the flexible polymer) of 51 nm (Fig. 5). Note that the exact evaluation of the length of the cylinder (above tens of nanometers) is not possible with $q > 5 \cdot 10^{-3}$ $Å^{-1}$. Furthermore, for $q > 0.1$ $Å^{-1}$, similar oscillations to those observed with the discrete **1.Co$^{II}$** and aggregated **1.Co$^{III}$** species in DMSO-$d_6$ solutions are present and indicate that all these aggregated species are composed of the metallomacrocyles, acting as secondary building units. The fact that in DMSO-$d_6$/$CD_3CN$ (1:4, vol/vol) mixtures **1.Co$^{II}$** and **1.Co$^{III}$** display different SAXS patterns indicate that the metallomacrocycles are differently organized in their aggregated forms. Transmission electron microscopy (TEM) of the supramolecular organization was performed after the deposition of a few drops of a solution of **1.Co$^{III}$** in a DMSO-$d_6$/MeCN (1:4 vol/vol) mixture on a Cu grid covered with an amorphous carbon film. Electron micrographs at high magnification show worm-like structures with variable lengths (up to 60 nm) and rather homogeneous width (5–7 nm) in agreement with SAXS (Fig. 6).

Some apparently multibranched nanoobjects are observed and possibly result from further aggregation of different nanostructures during deposition. Note that few ellipsoidal objects with length inferior to 10 nm are also present and may correspond to the small aggregates of **1.Co$^{III}$** in pure DMSO-$d_6$.

**Modification of the Solvent Composition: DMSO–$H_2O$ Mixtures.** We previously observed that the addition of water to a diluted solution of **1.Fe$^{II}$** in DMSO-$d_6$ system did not lead to precipitation while the starting hybrid **1** is fully insoluble in water (as almost all POM-based hybrids isolated as tetrabutyl ammonium salt). The intriguing and unexpected aqueous solubility of these systems led us to investigate the structural organization of both **1.Co$^{II}$** and **1.Co$^{III}$** in DMSO/water mixtures by SAXS and TEM. The SAXS patterns of **1.Co$^{III}$** ($c_{POM}$ = 1 mM) in DMSO-$d_6$/$H_2O$ (1:1, vol/vol) is very similar to that of **1.Co$^{III}$** in DMSO-$d_6$/$CD_3CN$ (1:4 vol/vol) mixture (*SI Appendix*, Fig. S6). The SAXS signal can be nicely fitted in the low-q region by a theoretical SAXS of flexible cylinder of similar dimensions (i.e., 3–3.6 nm in radius). Similarly, the SAXS curve of **1.Co$^{II}$** in DMSO-$d_6$/$H_2O$ (1:4, vol/vol) is similar to that of **1.Co$^{III}$** in DMSO-$d_6$/$CD_3CN$ or DMSO-$d_6$/$H_2O$ mixtures (*SI Appendix*, Fig. S7). This indicates that in the presence of an excess of water only the worm-like nanostructures are stabilized regardless of the charge of the metal linker. However, in a DMSO-$d_6$/$H_2O$ (1:1, vol/vol) mixture, the SAXS curve of **1.Co$^{II}$** ($c_{POM}$ = 1 mM) displays a different growth in the low-q region (*SI Appendix*, Fig. S7), suggesting the presence of smaller aggregates in such mixture. TEM micrographs of the nanoaggregates of **1.Co$^{II}$** and **1.Co$^{III}$** from DMSO-$d_6$/$H_2O$ (1:4, vol/vol) mixtures confirmed the formation of the worm-like nanostructures (*SI Appendix*, Fig. S8). The nanoobjects formed with the **1.Fe$^{II}$** system in DMSO-$d_6$/$CD_3CN$ mixtures were described as monodisperse nanoparticles (21). These nanoobjects result from the aggregation of the preformed metallomacrocycles through electrostatic interactions owing to the presence of the anionic (POMs) and cationic (metal linker and TBA) moieties within their structure. We noticed that these types of supramolecular architectures have a maximum compactness probably at the expense of electrostatic interactions (21). In the

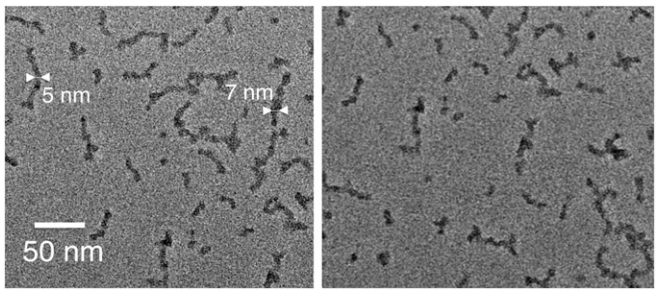


**Fig. 6.** Representative TEM micrographs of worm-like **1.Co$^{III}$** supramolecular organizations from a DMSO-$d_6$/MeCN solution.

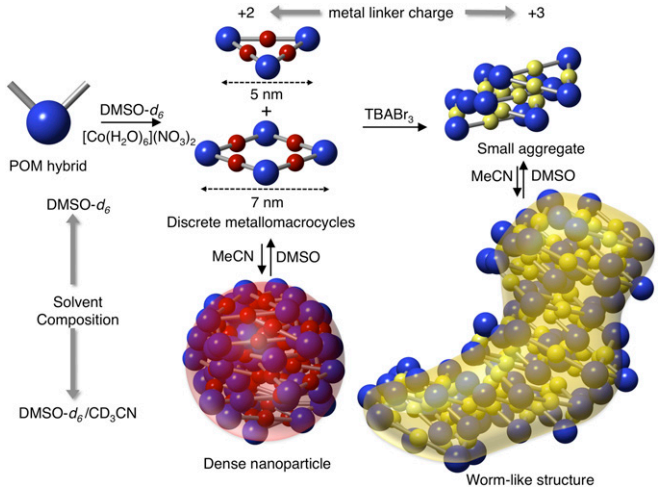


**Fig. 7.** Schematic representation of the formation of the nanosized aggregates by hierarchical metal-driven self-assembly of **1** according to the solvent composition (DMSO-$d_6$/$CD_3CN$ mixtures) and the metal linker charge. For sake of clarity the proposed structure of the small aggregates of **1.Co$^{III}$** (in DMSO) only contains molecular triangles.

present case the modification of the metal linker charge (or the addition of water) give rise to a type of supramolecular organization. Indeed, the increase of the metal linker charge strengthens the electrostatic interactions and thus initiates the aggregation even in DMSO-$d_6$. In DMSO-$d_6$/$CD_3CN$ mixtures, **1.Co$^{III}$** display worm-like structures. From SAXS and TEM micrographs the width of these structures is estimated to range between 5 and 7 nm. Interestingly, these values match the dimensions of energy-minimized structures of the molecular triangle and square (Fig. 7) (21). We propose that the **1.Co$^{III}$** worm-like structures arise from a stacking of the macrocycles along a preferential direction. This aggregation mode would favor electrostatic interactions between the metallomacrocycles at the expense of a lower compacity compared with the previously reported nanoparticles of **1.Fe$^{II}$**. Fits of the SAXS signals of **1.Co$^{III}$** in DMSO-$d_6$/$CD_3CN$ (1:4, vol/vol) using a core shell cylinder model were tried but the calculated SAXS patterns did not satisfactory reproduce the experimental SAXS features in the intermediate (~$10^{-1}$ $Å^{-1}$) region. Consequently, it is unlikely that in the aggregated species of **1.Co$^{III}$** in DMSO-$d_6$/$CD_3CN$ (1:4, vol/vol), the metallomacrocycles would stack in a columnar arrangement with the organic arms forming a hydrophobic channel. It is more likely that the metallomacrocycles would perform a tilted stacking such as exemplified in Fig. 7, forming thus an oblique cylinder. Molecular dynamics of the aggregation processes using simple point-charge models should be useful to investigate in more detail what are the most favorable aggregation modes. While the metallomacrocycles are mixtures of molecular triangles and squares, the mismatch between these two species would lead to defects in the stacking of the metallomacrocycles, generating the worm-like structures (Fig. 7). We can observe that the discrete metallomacrocycles display amphiphilic character owing to the presence of the hydrophilic POMs, hydrophobic organic moieties, and amphiphilic TBA cations. As the section of the worm-like assemblies (5–7-nm diameter) roughly corresponds to that of the discrete metallomacrocycles, it is likely that in this nanoorganization, POMs mostly point toward the solvent. In contrast, in the dense nanoaggregates a number of POMs are buried inside the aggregate, the diameter of the nanoparticles being bigger than the POM-to-POM distance within the metallomacrocycles. The worm-like nanostructures would then preferentially form in the presence of water owing to improved interactions between the charged POMs and TBA with water.

**Molecular Carrier Properties.** The assemblies **1.Co$^{II}$** and **1.Co$^{III}$** are soluble upon dilution with water and both form similar worm-like structures. Owing to the emergent water solubility of these nanoaggregates we investigated, in a preliminary study, their ability to act as molecular carrier. Pyrene derivatives are well-known polyaromatic compounds that are almost insoluble in DMSO/$H_2O$ mixtures. When a DMSO-$d_6$ solution of the preformed **1.Co$^{II}$** and **1.Co$^{III}$** species ($c_{POM}$ = 0.5 mM) containing a very large excess of 1-bromopyrene is diluted with water, an instant precipitation of the 1-bromopyrene and the POM-based assemblies occurs, producing a colorless solution. However, for solutions containing 10 equiv (or less) of 1-bromopyrene per POM ($c_{POM}$ = 0.5 mM) in DMSO-$d_6$, only a slight, almost colorless precipitate (corresponding to excess of 1-bromopyrene) forms upon dilution with water. UV-vis spectra of **1.Co$^{II}$** and **1.Co$^{III}$** in DMSO:$H_2O$ (2:98, vol/vol, $c_{POM}$ = 10 μM) mixtures were recorded after filtration of the solution through a polytetrafluoroethylene membrane (0.45 μm). Above 350 nm, the spectra are dominated by the cobalt bis(terpyridine) absorption since the POM only contributes to the intense absorption below 300 nm (*SI Appendix*, Fig. S9). When 1-bromopyrene (10 equiv per POM) was added to the POM-based assemblies in DMSO, the UV-vis spectra of the solution obtained after dilution with water (yielding DMSO:$H_2O$ (2:98, vol/vol) mixtures, $c_{POM}$ = 10 μM) and filtration on a PTFE membrane, clearly indicate the presence of 1-bromopyrene (with characteristic absorption features at 280 and 340 nm) with a slight decrease in the global absorption (compared with spectra of pure **1.Co$^{II}$** and **1.Co$^{III}$** in DMSO-$d_6$:$H_2O$ mixtures with the same initial concentration of POMs), the absorption solution remaining then stable for few hours (Fig. 8). While the absorption decrease of the solution is almost null for **1.Co$^{III}$** (3% signal loss at λ = 400 nm), it is more pronounced for **1.Co$^{II}$** (24% signal loss at λ = 400 nm), suggesting that **1.Co$^{II}$** is more prone to precipitation than **1.Co$^{III}$** in the presence of hydrophobic species. After subtraction of the absorbance of the POM-based assemblies, the calculated absorbance at 337 nm (maximum absorption of the 1-bromopyrene) is ΔA = 0.27 and ΔA = 0.48 for solutions of **1.Co$^{II}$** and **1.Co$^{III}$**, respectively. In DMSO, 1-bromopyrene displays a maximum absorption at 332 nm with an extinction coefficient $\varepsilon_{332} = 3.6 \times 10^4$ $M^{-1}$ $cm^{-1}$(*SI Appendix*, Fig. S10). Considering that this ππ* transition is only slightly affected by the solvent composition this would give a concentration

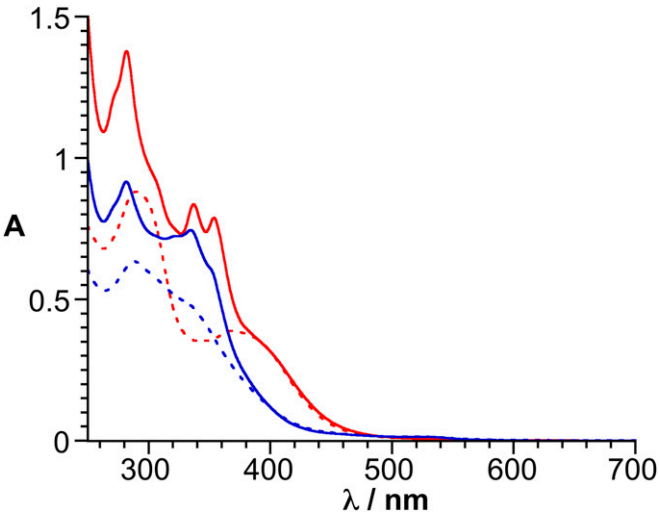


**Fig. 8.** UV-vis absorption spectra of solutions of **1.Co$^{II}$** (plain blue) and **1.Co$^{III}$** (plain red) containing 1-bromopyrene in DMSO-$d_6$/$H_2O$ mixtures (2:98, vol/vol, $c_{POM} = 10^{-5}$ M). Dotted lines correspond to spectra of solutions of **1.Co$^{II}$** (blue) and **1.Co$^{III}$** (red) in DMSO-$d_6$:$H_2O$ (2:98) (a correction factor is applied to the dotted spectra to account for the slight decrease in absorption of the solutions containing 1-bromopyrene).

of ~7.5 and 13 μM of 1-bromopyrene for solutions containing **1.Co$^{II}$** and **1.Co$^{III}$**, respectively, i.e., similar concentrations to that of the POMs. As a non-negligible amount of **1.Co$^{II}$** is removed by filtration on the PTFE membrane in the presence of 1-bromopyrene, the lower incorporation of 1-bromopyrene with this system may in part arise from the lower solubility of the resulting assembly. Finally, TEM micrographs of the nanoaggregates of **1.Co$^{II}$** and **1.Co$^{III}$** containing 1-bromopyrene in DMSO-$d_6$/$H_2O$ mixtures show the presence of the worm-like nanostructures (*SI Appendix*, Fig. S11) indicating that the presence of 1-bromopyrene in the nanoaggregates does not significantly modify the supramolecular architecture. However, it can be noted that for **1.Co$^{II}$** a significant number of smaller aggregates is observed. The formation of such smaller aggregates with **1.Co$^{II}$** in the presence of 1-bromopyrene may also accounts for the lower incorporation of the polyaromatic guest. Owing to the well-known bioactivity of POMs (33–35), these aqueous soluble nanoobjects further displaying molecular carrier properties (drug delivery) hold great promise for biological applications.

## Conclusion

We showed that the POM-based building unit **1** can give access to multiscale nanoarchitectures through metal-driven self-assembly processes. Different nanoorganizations can be selectively formed according to the solvent composition and the charge of the metal linker. These two parameters modulate the electrostatic interactions between the metallomacrocycles, acting as secondary building units, and constitute control levers of the formation of the hierarchical supramolecular architectures. In pure DMSO-$d_6$ we observed the minor presence of molecular squares, which could not be identified in a previous study (21). In DMSO-$d_6$/$CD_3CN$ mixtures, when the metallomacrocycle is connected by a divalent transition metal ($Fe^{II}$ or $Co^{II}$) the nanoaggregates display nanoparticle-like structures. In these highly compact nanoassemblies the metallomacrocyles building units have probably no specific orientation. By contrast with a trivalent metal linker ($Co^{III}$) the aggregation of the metallomacrocycle occurs along a preferential orientation owing to increased electrostatic interactions yielding the worm-like assemblies. These structures were also observed in DMSO-$d_6$/$H_2O$ mixtures whether with divalent or trivalent metal linkers probably since they optimize the interactions of the POMs (and TBA cations) with water. The emergent aqueous solubility of the nanoaggregates drove us to explore the ability of these systems to act as molecular carriers. We observed that in both cases the supramolecular assemblies allow dissolving polyaromatic guests at concentrations similar to those of the starting POM-based building blocks. This opens the way to potential applications of these nanoobjects for chemical biology.

## Materials

Compound **1** was prepared according to a published procedures (22). All other reagents were used as supplied. The preparation of the supramolecular species **1.Co$^{III}$** always relies on the prior formation of **1.Co$^{II}$** in DMSO-$d_6$ followed by its oxidation through the addition of 1 equiv $TBABr_3$.

**ACKNOWLEDGMENTS.** We thank Javiez Perez for assistance in using beamline SWING. We thank François Ribot for kind help with $T_2$ measurements. We acknowledge SOLEIL Synchrotron for providing beamtime and synchrotron radiation facilities. This work benefited from the use of the SasView application, originally developed under NSF award DMR-0520547. SasView contains code developed with funding from the European Union's Horizon 2020 research and innovation programme under the SINE2020 project, Grant Agreement 654000. This work was supported by the French National Research Agency (EXPAND Project Grant ANR 14-CE08-0002).

1. Babloyantz A (1986) *Molecules, Dynamics, and Life: An Introduction to Self-Organization of Matter* (John Wiley & Sons, New York).
2. Lescop C (2017) Coordination-driven syntheses of compact supramolecular metallacycles toward extended metallo-organic stacked supramolecular assemblies. *Acc Chem Res* 50:885–894.
3. Keizer HM, Sijbesma RP (2005) Hierarchical self-assembly of columnar aggregates. *Chem Soc Rev* 34:226–234.
4. Yan Y, Huang JB (2010) Hierarchical assemblies of coordination supramolecules. *Coord Chem Rev* 254:1072–1080.
5. Rest C, Kandanelli R, Fernández G (2015) Strategies to create hierarchical self-assembled structures via cooperative non-covalent interactions. *Chem Soc Rev* 44:2543–2572.
6. Mariani G, Moldenhauer D, Schweins R, Gröhn F (2016) Elucidating electrostatic self-assembly: Molecular parameters as key to thermodynamics and nanoparticle shape. *J Am Chem Soc* 138:1280–1293.
7. Kim Y, Li W, Shin S, Lee M (2013) Development of toroidal nanostructures by self-assembly: Rational designs and applications. *Acc Chem Res* 46:2888–2897.
8. Yu G, Jie K, Huang F (2015) Supramolecular amphiphiles based on host-guest molecular recognition motifs. *Chem Rev* 115:7240–7303.
9. Luisi P (2002) Emergence in chemistry: Chemistry as the embodiment of emergence. *Found Chem* 4:183–200.
10. Yan X, et al. (2013) Supramolecular polymers with tunable topologies via hierarchical coordination-driven self-assembly and hydrogen bonding interfaces. *Proc Natl Acad Sci USA* 110:15585–15590.
11. Northrop BH, Zheng YR, Chi KW, Stang PJ (2009) Self-organization in coordination-driven self-assembly. *Acc Chem Res* 42:1554–1563.
12. Han M, Engelhard DM, Clever GH (2014) Self-assembled coordination cages based on banana-shaped ligands. *Chem Soc Rev* 43:1848–1860.
13. Rubinstein M, Papoian GA (2012) Polyelectrolytes in biology and soft matter. *Soft Matter* 8:9265–9267.
14. Doni G, Kostiainen MA, Danani A, Pavan GM (2011) Generation-dependent molecular recognition controls self-assembly in supramolecular dendron-virus complexes. *Nano Lett* 11:723–728.
15. Yan Y, Huang JB (2010) Hierarchical assemblies of coordination supramolecules. *Coord Chem Rev* 254:1072–1080.
16. Kurth DG, Higuchi M (2006) Transition metal ions: Weak links for strong polymers. *Soft Matter* 2:915–927.
17. Tian Y, Yan X, Saha ML, Niu Z, Stang PJ (2016) Hierarchical self-assembly of responsive organoplatinum(II) metallacycle-TMV complexes with turn-on fluorescence. *J Am Chem Soc* 138:12033–12036.
18. Chen LJ, et al. (2015) Hierarchical self-assembly of discrete organoplatinum(II) metallacycles with polysaccharide via electrostatic interactions and their application for heparin detection. *J Am Chem Soc* 137:11725–11735.
19. Yan X, et al. (2013) Hierarchical self-assembly: Well-defined supramolecular nanostructures and metallohydrogels via amphiphilic discrete organoplatinum(II) metallacycles. *J Am Chem Soc* 135:14036–14039.
20. Piot M, et al. (2017) Charge effect on the formation of polyoxometalate-based supramolecular polygons driven by metal coordination. *Inorg Chem* 56:8490–8496.
21. Izzet G, et al. (2016) Hierarchical self-assembly of polyoxometalate-based hybrids driven by metal coordination and electrostatic interactions: From discrete supramolecular species to dense monodisperse nanoparticles. *J Am Chem Soc* 138:5093–5099.
22. Izzet G, et al. (2015) Metal-directed self-assembly of a polyoxometalate-based molecular triangle: Using powerful analytical tools to probe the chemical structure of complex supramolecular assemblies. *Chemistry* 21:19010–19015.
23. Izzet G, Volatron F, Proust A (2017) Tailor-made covalent organic-inorganic polyoxometalate hybrids: Versatile platforms for the elaboration of functional molecular architectures. *Chem Rec* 17:250–266.
24. Song YF, Tsunashima R (2012) Recent advances on polyoxometalate-based molecular and composite materials. *Chem Soc Rev* 41:7384–7402.
25. Matt B, et al. (2011) Hybrid polyoxometalates: Keggin and Dawson silyl derivatives as versatile platforms. *J Org Chem* 76:3107–3112.
26. Nomiya K, et al. (2011) Synthesis and structure of Dawson polyoxometalate-based, multifunctional, inorganic-organic hybrid compounds: Organogermyl complexes with one terminal functional group and organosilyl analogues with two terminal functional groups. *Inorg Chem* 50:9606–9619.
27. Aoki S, Kurashina T, Kasahara Y, Nishijima T, Nomiya K (2011) Polyoxometalate (POM)-based, multi-functional, inorganic-organic, hybrid compounds: Syntheses and molecular structures of silanol- and/or siloxane bond-containing species grafted on mono- and tri-lacunary Keggin POMs. *Dalton Trans* 40:1243–1253.
28. Chambers J, et al. (2006) Inductive influence of 4′-terpyridyl substituents on redox and spin state properties of iron(II) and cobalt(II) bis-terpyridyl complexes. *Inorg Chim Acta* 359:2400–2406.
29. McQueen EW, Goldsmith JI (2009) Electrochemical analysis of single-walled carbon nanotubes functionalized with pyrene-pendant transition metal complexes. *J Am Chem Soc* 131:17554–17556.
30. Nyman M (2017) Small-angle X-ray scattering to determine solution speciation of metal-oxo clusters. *Coord Chem Rev* 352:461–472.
31. Li M, Wang W, Yin P (2018) A general approach to access morphologies of polyoxometalates in solution by using SAXS: An ab initio modeling protocol. *Chemistry* 24:6639–6644.
32. Als-Nielsen J, McMorrow D (2001) *Elements of Modern X-Ray Physics* (Wiley, New York).
33. Gao P, Wu Y, Wu L (2016) Co-assembly of polyoxometalates and peptides towards biological applications. *Soft Matter* 12:8464–8479.
34. Ly HGT, Absillis G, Janssens R, Proost P, Parac-Vogt TN (2015) Highly amino acid selective hydrolysis of myoglobin at aspartate residues as promoted by zirconium(IV)-substituted polyoxometalates. *Angew Chem Int Ed Engl* 54:7391–7394.
35. Wille H, et al. (2009) Surface charge of polyoxometalates modulates polymerization of the scrapie prion protein. *Proc Natl Acad Sci USA* 106:3740–3745.
36. SasView (2017) Small Angle Scattering Analysis Software Package. Available at www.sasview.org/. Accessed August 15, 2017.